A Kinetic Model of the Formation of Organic Monolayers on Hydrogen-Terminated Silicon by Hydrosilation of Alkenes

M. Woods, S. Carlsson, Q. Hong, S. N. Patole, L. H. Lie, A. Houlton, and B. R. Horrocks*

School of Natural Sciences: Chemistry, University of Newcastle upon Tyne, Newcastle upon Tyne NE1 7RU, U.K.

Received: May 14, 2005; In Final Form: October 12, 2005

We have analyzed a kinetic model for the formation of organic monolayers based on a previously suggested free radical chain mechanism for the reaction of unsaturated molecules with hydrogen-terminated silicon surfaces (Linford, M. R.; Fenter, P. M.; Chidsey, C. E. D. *J. Am. Chem.* Soc **1995**, *117*, 3145). A direct consequence of this mechanism is the nonexponential growth of the monolayer, and this has been observed spectroscopically. In the model, the initiation of silyl radicals on the surface is pseudo first order with rate constant, k_i, and the rate of propagation is determined by the concentration of radicals and unreacted Si−H nearest neighbor sites with a rate constant, k_p. This propagation step determines the rate at which the monolayer forms by addition of alkene molecules to form a track of molecules that constitute a self-avoiding random walk on the surface. The initiation step describes how frequently new random walks commence. A termination step by which the radicals are destroyed is also included. The solution of the kinetic equations yields the fraction of alkylated surface sites and the mean length of the random walks as a function of time. In mean-field approximation we show that (1) the average length of the random walk is proportional to $(k_p/k_i)^{1/2}$, (2) the monolayer surface coverage grows exponentially only after an induction period, (3) the effective first-order rate constant describing the growth of the monolayer and the induction period (kt) is $k = (2k_ik_p)^{1/2}$, (4) at long times the effective first-order rate constant drops to k_i, and (5) the overall activation energy for the growth kinetics is the mean of the activation energies for the initiation and propagation steps. Monte Carlo simulations of the mechanism produce qualitatively similar kinetic plots, but the mean random walk length (and effective rate constant) is overestimated by the mean field approximation and when $k_p \gg k_i$, we find $k \sim k_i^{0.7}k_p^{0.3}$ and $E_a = (0.7E_i + 0.3E_p)$. However the most striking prediction of the Monte Carlo simulations is that at long times, $t \gg 1/k$, the effective first-order rate constant decreases to k_i even in the absence of a chemical termination step. Experimental kinetic data for the reaction of undec-1-ene with hydrogen-terminated porous silicon under thermal reflux in toluene and ethylbenzene gave a value of $k = 0.06$ min^{-1} and an activation energy of 107 kJ mol^{-1}. The activation energy is in reasonable agreement with density functional calculations of the transition state energies for the initiation and propagation steps.

Introduction

The formation of organic monolayers on hydrogen-terminated silicon by hydrosilation of unsaturated molecules leads to robust Si−C bonded organic monolayers.[1−5] The hydrosilation reaction can be driven thermally,[2,6−9] photochemically[10−16] by catalysts,[17−20] electrochemically,[21,22] or by a scanning tunneling microscope tip to form molecular lines.[23−27] These monolayers have become useful for a range of investigations because the chemistry is compatible with many functional groups,[4,5,13,20,28,29] because the monolayers can be well-ordered,[9,30−38] and because they provide access to an alternative substrate (crystalline silicon) to the well-established thiolate self-assembled monolayers (SAMs) on gold.[39] The same class of hydrosilation reactions also allows formation of organic monolayers on porous silicon[3,7,40−43] and silicon quantum dots.[44−48]

The mechanism of the hydrosilation reaction, in which the surface Si−H bond adds across the unsaturated carbon−carbon bonds, was originally proposed to be a radical mechanism.[2] This mechanism is widely accepted for thermal and photochemical initiation of the reaction.[4,5] Tests of the mechanism have included the use of deuterium labeling to follow the fate of the hydrogen atoms on the silicon surface[49−51] and direct observations of the early stages of monolayer formation by probe microscopy.[15,23,52,53] There is now strong evidence that the mechanism is correct for styrene reacting with Si(111)−H and Si(100)−H,[5] vinylferrocene with Si(100),[54] and alkenes longer than heptene on Si(100).[53] Some contrary results have been obtained for propene/Si(100)−H[5,53] and undecene/abraded Si(111)−H:[50] these results may indicate a relatively small barrier to desorption of the alkyl radical (especially in ultrahigh vacuum) compared to the activation energy for hydrogen abstraction to form new silyl radicals and propagate the chain.[55] However other explanations for some of these data[50] have been suggested.[5] Although it is not possible to obtain direct probe microscopic evidence, FTIR studies also suggest that the same mechanism applies on hydrogen-terminated porous silicon surfaces.[49,51] To date relatively few kinetic studies of the mechanism have been made.[33,56,57] These studies found first-order kinetics, with an exponential growth of the surface coverage, on porous silicon[56] and single-crystal wafers.[33,57] A related type of monolayer, generated electrochemically by

* To whom correspondence should be addressed: E-mail: b.r.horrocks@ncl.ac.uk.

10.1021/jp052542e CCC: $30.25
Published on Web 11/25/2005

radicals formed during electrooxidation of Grignard reagents, has been analyzed kinetically, but the mechanism is rather different and does not have the same radical chain propagation characteristics.[58] In this paper we report a theoretical treatment of the radical chain mechanism (2) for the hydrosilation reaction of hydrogen-terminated silicon and some kinetic measurements which explore some novel consequences of the mechanism. We show that the mechanism provides natural explanations for aspects of the existing kinetic data[33] that were not accounted for by a simple first-order rate law.

Experimental Section

Materials. All reagents and solvents were obtained from Sigma/Aldrich and were of AnalaR grade or comparable. Toluene and ethylbenzene were dried over Na and distilled before use. Si wafers were obtained from Compart Technology, Cambridge, U.K., and the particular specifications are given below.

Preparation of Hydrogen-Terminated Porous Silicon for FTIR Analysis. Si wafers (⟨100⟩ oriented; boron-doped, p-type, 5−15 Ω cm resistivity) were degreased in acetone. The oxide was removed from one side by abrasion, and a thin In/Ga film or Al foil was applied to ensure a good contact with the electrode. The sample was held in a Teflon cell between two Viton O-rings and hydrogen-terminated porous silicon (PS−H) was formed by galvanostatic anodization in a 1:1 v/v solution of 48% aqueous HF to ethanol. A current of 10 mA was applied for 5 min, and the wetted area of the sample was 0.785 cm^2 (diameter = 1 cm). These etching conditions were chosen to produce highly uniform PS layers, that are stable under the reaction conditions used for the hydrosilylation, and to minimize cracking of the porous layer, rather than to optimize other properties such as luminescence. The porous silicon was then rinsed in deionized water (Millipore, 18 MΩ cm), immersed in 48% aqueous HF, rinsed in deionized water, and dried in a stream of dry nitrogen.

Infrared Spectroscopy. Spectra (unpolarized, normal transmission) were obtained using a Bio-Rad Excalibur spectrometer with an MCT detector. Spectra of both alkylated and unmodified porous silicon were referenced against an unetched piece of Si(100) wafer and have been baseline-corrected with the instrument-supplied (Merlin) software. The resolution was 4 cm^{-1}, and 32 scans have been coadded and averaged. The integrated peak intensity, denoted as A, was calculated by using the integration facility of the same software. To achieve reproducible data during kinetic runs, the sample was mounted in the spectrometer on a steel plate with a circular hole (0.5 cm diameter) for the infrared beam to pass through the sample. Marks scored on the steel enabled the sample to be placed in the same orientation and location in the beam throughout a kinetic run in which multiple spectra were recorded on a single porous silicon sample. By restriction of the area examined by FTIR to a circular region of diameter 0.5 cm in the center of each chip, the precision was improved because the porous layer is more homogeneous in the center than at the perimeter of the etched area.

Protocol for the Kinetic Investigation of Monolayer Formation on Porous Silicon by FTIR Spectroscopy. To obtain a sufficient number of data points and precision for a detailed kinetic analysis, a single chip was employed to generate each absorbance−time curve from which a rate constant at the given temperature was extracted. Since it was not possible to carry out the FTIR spectroscopy during the reflux, the chip was removed from the reaction flask several times to record a spectrum ex situ and then immersed again in the refluxing reaction mixture (10 mL solvent, 100 mM undecene). The reaction times reported therefore correspond to the accumulated time spent by the chip at reflux in the reaction flask. To check that the repeated emersion of the chip does not affect the progress of the reaction, a few experiments were conducted in which the absorbance spectra of chips left undisturbed in the reaction flask for an equivalent time were compared with those which had been emersed at 5 min intervals. It was found possible to make any difference insignificant by arranging that the chip was washed with pure solvent (toluene) immediately upon emersion and blown dry with N_2 and the spectrum recorded before reimmersion within ca. 10 min in a reaction mixture that was *kept at reflux* to ensure that there was no significant delay due to heating/cooling of the liquid.

Data as a function of reaction temperature were obtained by using solvent mixtures to vary the normal boiling point. Toluene and ethylbenzene were chosen as the solvents to give a range of temperatures of ca. 111−136 °C; these solvents form an almost ideal mixture. Although other solvents could be used to extend this range, it was found that for temperatures below that of the toluene boiling point difficulties in obtaining precise spectroscopic data arise from the long reaction times and for higher boiling solvents, e.g., mesitylene, it was not possible to obtain the data rapidly enough.

Computational Methods. All DFT calculations were carried out using the PC-GAMESS version[59] of the GAMESS-US program.[60] The saddle point and reactant geometries were optimized without any symmetry assumptions using the B3LYP functional as implemented in Gaussian 98, i.e., using the keyword B3LYP1 and with a 6-31G(d,p) basis set. Both spin-restricted (ROHF) and spin-polarized (UHF) calculations were carried out. To model the initiation step, calculations were made with an oxygen molecule ($S = 2$) placed close to one of the hydrogen atoms of a Si_6H_{12} cluster. The equilibrium geometry of the reactant and the saddle points were confirmed by vibrational calculations at the same level of theory. No scale factor was employed for the zero point vibrational energies because the recommended values for the functional and basis set used are so close to unity.[61] No attempt was made to correct for basis set superposition errors.

Results and Discussion

This paper is organized in four sections: first the kinetic model is described; the model is then solved in mean-field approximation and then the same model is solved by Monte Carlo simulation; next, experimental evidence for the model from kinetic experiments using FTIR spectroscopy of porous silicon is discussed; and finally, the Arrhenius' law activation energy of the reaction is compared to quantum chemical calculations of small molecule models of the transition states.

Kinetic Model. The radical chain mechanism for the hydrosilation reaction of alkenes by hydrogen-terminated silicon surfaces we analyze in this report is based on that of Linford et al.[2]:

k_i initiation

$$\mathrm{Si{-}H} \rightarrow \mathrm{Si^{\bullet}} \qquad (1)$$

k_a addition

$$\mathrm{Si^{\bullet} + H_2C{=}CH{-}R} \rightarrow \mathrm{Si{-}CH_2{-}CH^{\bullet}{-}R} \qquad (2)$$

k_p propagation

$$Si{-}CH_2{-}CH^{\bullet}{-}R + Si{-}H \rightarrow Si{-}CH_2{-}CH_2{-}R + Si^{\bullet} \quad (3)$$

k_t termination

$$Si{-}CH_2{-}CH^{\bullet}{-}R + Solv{-}H \rightarrow Si{-}CH_2{-}CH_2{-}R + Solv^{\bullet} \quad (4)$$

Si stands for a single silicon atom on the surface, Si−H is a surface hydrogen atom available for hydrosilation, and Si• is a silyl radical. This model was based on analogies with molecular organosilane chemistry but is now supported by experimental evidence from high-resolution probe microscopy on single-crystal material (review in ref 5) and by deuterium labeling studies on porous silicon.[49,51] However, a full kinetic analysis has not yet been made.

The closest previously reported mechanistic analysis to this work, is for the adsorption of undecene on Si(100) in a vacuum.[57] Those authors include our steps 2 and 3 above and treat a case where (in our terminology) $k_i = 0$, $k_t = 0$ and there is a small, constant number of radicals on the surface. They observe first-order kinetics (exponential growth of the surface coverage) in a steady-state approximation appropriate for the data obtained during reaction in a vacuum. In this report we treat explicitly the kinetics of initiation and termination and consider cases where k_p may be large and the interesting phenomena of self-directed growth of lines[53] or self-avoiding random walks occur.[10] Before attempting to calculate the growth kinetics of the monolayer according to the mechanism, we discuss each elementary step in the mechanism in turn.

Reaction 1 is the initiation of a radical chain process, and since the reaction may be driven photochemically[10−16] the rate constant k_i may be a pseudo rate constant dependent on the light intensity. In the case of a thermally driven reaction, the initiation step is likely to involve another chemical species because the Si−H bond energy on the surface (330−350 kJ mol^{-1} [62,63]) is too large for this to occur by simple dissociation at the rates and temperatures observed on porous silicon (refluxing toluene, time scales of 30 min to 1 h). Instead we suggest that trace oxygen abstracts a hydrogen atom

$$Si{-}H + O_2 \rightarrow Si^{\bullet} + HO_2^{\bullet} \quad (5)$$

In this case k_i is also a pseudo rate constant with a value proportional to the oxygen concentration, $k_i = k_{i2}[O_2]$. We have recently reported experimental evidence that oxygen molecules are involved in the thermal hydrosilation.[51]

After the initiation step, an alkene molecule adds to the silyl radical (2) and a propagation step can occur (3), in which the radical on the β-carbon abstracts a nearest-neighbor hydrogen atom to generate another silyl radical. Another addition step follows, and the process continues leaving a track of alkylated sites across the surface that constitutes the random walk discussed below. Throughout the text we use the term random walk to indicate the track of reacted alkyl sites formed by the propagation step whether it is in fact random or not. The overlap of these random walks eventually leads to the formation of a monolayer.

In principle the rate is dependent on the alkene concentration, e.g., for the sequential combination of initiation and addition steps

$$\frac{1}{\text{rate}} = \frac{1}{k_{i2}[O_2][Si{-}H]} + \frac{1}{k_a[\text{alkene}][Si^{\bullet}]} \quad (6)$$

However, since our previous data (ref 56) shows only a weak dependence of the kinetics on [alkene], i.e., a small decrease in rate for a 10-fold increase in [alkene], we assume throughout that the addition steps are fast. The rate-determining steps therefore correspond to the initiation and propagation above and are described by k_i and k_p.

We have ignored bimolecular termination processes since the radicals are covalently attached to the surface and immobile. It is possible that two radicals, which are nearest neighbors, form a carbon−carbon bond, but we assume this process is rare on grounds of concentration. The absence of bimolecular termination and the confinement of the growing polymer chains to fixed sites on the surface are the main differences between this mechanism and the well-known Flory mechanism of free radical polymerization in solution. There are, however, some similarities with phenomena associated with the "gel effect" in free radical polymerization: When the volume fraction of polymer becomes large, the viscosity of the solution increases and the diffusion of radicals and the rate of recombination of radicals slows.[64] On the surface, diffusion of the covalently bound radicals is less likely still and therefore we make the approximation that it does not take place at all.

If we write n for the fraction of surface sites containing a carbon radical (Si−CH$_2$−CH•−R) and s for the fraction of unreacted Si−H sites, the kinetic equations in mean field approximation are

$$\frac{dn}{dt} = k_i s - k_t n \quad (7)$$

and

$$\frac{ds}{dt} = -k_i s - k_p n s \quad (8)$$

and the boundary conditions are $s(t=0) = 1$ and $n(t=0) = 0$. Previous workers have treated the propagation steps of this system as a self-avoiding random walk and showed that such a process terminates naturally when the radical is surrounded by nearest neighbor sites that have already reacted.[10] We treat this effect by Monte Carlo simulations below. Such a termination process could also be modeled crudely by a kinetic term proportional to the mole fractions of radicals and reacted sites, $-k_t n(1 - s)$, in eq 7: this case is treated by a linear approximation in the Appendix. Equations 7 and 8 do however capture the main effect of having multiple random walks occurring on the surface, which is to reduce the mean random walk length compared to that (76 steps) for an isolated walk on the Si(111) surface[10] because the available surface sites become exhausted.

The mean-field formulation also ignores certain aspects of the problem relating to the geometry of the lattice, i.e., as the surface coverage approaches a full monolayer, some new radicals may be initiated in small holes in the monolayer where they are surrounded by reacted sites. These radicals cannot propagate to attain the same mean walk length as would be observed at low coverages where there are relatively few, widely spaced random walks which do not interfere with one another. These aspects are ignored in eqs 7 and 8 above and are treated instead by a Monte Carlo simulation: their major effect is on the long-time behavior of the reaction.

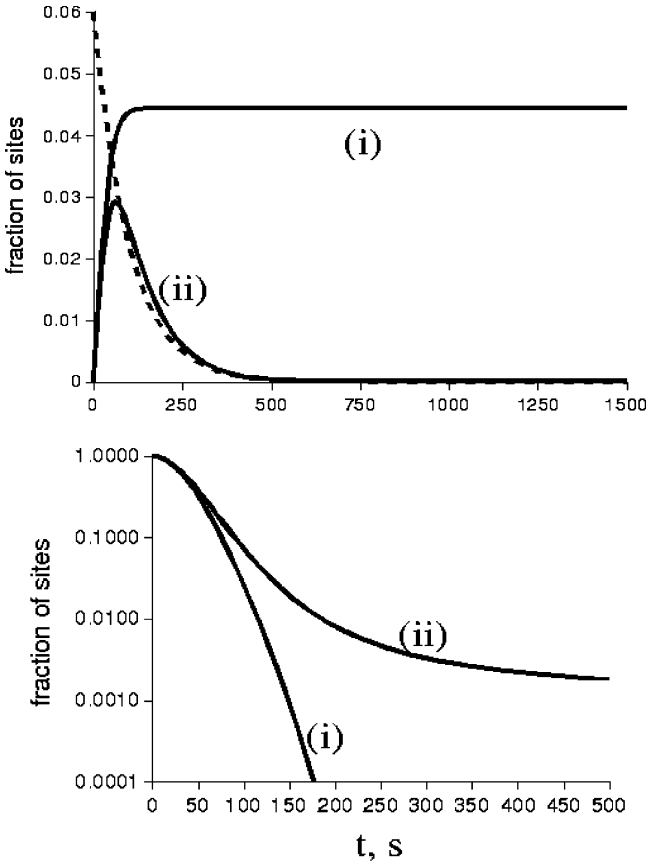

Figure 1. Finite difference solution of eqs 7 and 8 for n (top) and ln s (bottom). In both graphs $k_i = 10^{-3}$ s^{-1} and $k_p = 1.0$ s^{-1}. The termination rate constants are (i) $k_t = 0$ and (ii) $k_t = 10^{-2}$ s^{-1}. The dashed line (top) is a guide to the eye which shows the exponential decay of n at long times, $n \sim \exp(-k_i t)$.

50% Rule. It is generally accepted that steric factors restrict the coverage of long chain alkyl monolayers on hydrogen-terminated silicon to about 50% of the Si−H sites at the surface.[65] Recent quantitative photoemission studies have confirmed this expectation.[66] In the mean-field treatment, we could take account of this simply by defining the fractional surface coverage, s, in terms of the ca. 50% of Si−H sites actually accessible and the whole of the mathematical analysis and conclusions remain unchanged. The calculations at this level of approximation are therefore valid for any limit on the fractional surface coverage. In the case of Si(100) surfaces where available experimental evidence suggests the random walks are confined to rows of Si atoms,[23] the same comment applies to the Monte Carlo simulations because one could leave 50% of the rows unreacted. However the case of Monte Carlo simulation of Si(111) is more difficult, because the random walk can wander across the surface in two dimensions, and we would need to know in advance either the final arrangement of the molecules on the surface or an appropriate algorithm to determine which sites are sterically accessible. We are investigating such algorithms, but it is worth noting here that they constitute an extension of the basic model: the purpose of the present work is to analyze the consequences of the mechanism 1−4.

Kinetic Model. Mean Field Treatment. We have only obtained an exact solution of eqs 7 and 8 when $k_t = 0$. The full model can be easily solved numerically (Figure 1), and also asymptotic expressions were obtained by linearizing the equations (Appendix). Closed-form solutions are given below for several limiting cases.

Case I: Rapid Termination Kinetics. For rapid termination kinetics, $k_t \gg k_i$, the usual steady-state approximation for n in eq 7 may be applied

$$n_{ssa} = \frac{k_i s}{k_t} \tag{9}$$

Under this assumption, the solution for the fraction of unreacted sites, s, is

$$s = \frac{k_i e^{-k_i t}}{k_i + k_{ssa}(1 - e^{-k_i t})} \tag{10}$$

where $k_{ssa} = k_i k_p / k_t$. For $k_{ssa} \ll 1$ or $k_i t \gg 1$, the solution is well approximated by a simple exponential, and the effective first-order rate constant obtained from the usual semilogarithmic plot is k_i, the initiation rate constant. Also, the mean random walk length $\langle L \rangle$, expressed as the number of sites reacted for one initiation event, is given by the ratio of the propagation to termination rates plus 1

$$\langle L \rangle = \frac{k_p s}{k_t} + 1 \tag{11}$$

This case is of lesser interest experimentally because it describes the situation where each molecule that bonds to the surface requires a separate initiation event, i.e., the random walk length ∼1. However, case I may describe those experimental situations where there is evidence that the propagation step (reaction) is slow relative to the rate of termination.[5,50] In contrast, when k_t is small (cases II and III below) the molecules will tend to add to the end of a growing chain via reactions 2 and 3 which allows for steric and electronic factors to influence the relative orientation of the molecules and therefore affect the structure of the monolayer.

Case II: Zero Rate of Termination. When there is no chemical termination step, the mean walk length determined from eqs 7 and 8 still remains finite because at long times the available surface sites are exhausted. Since n is the fraction of surface sites that correspond to the head of a growing chain and $1 - s$ is the fraction of sites that have reacted, the mean length of a random walk (expressed in terms of the number of sites in the walk) is $\langle L \rangle = (1 - s)/n$. At long times $s \rightarrow 0$ and the mean walk length tends to $1/n_\infty$. For this case, which is of more interest experimentally, an exact solution to the kinetic equations is available[67] and an expression for the mean walk length at long times is also given below

$$\frac{n}{n_\infty} = \frac{1 - e^{-kt}}{1 + \frac{k - k_i}{k + k_i} e^{-kt}} \tag{12}$$

$$\frac{k_i s}{n_\infty} = k \frac{\left(1 + \frac{k - k_i}{k + k_i}\right) e^{-kt}}{\left[1 + \frac{k - k_i}{k + k_i} e^{-kt}\right]^2} \tag{13}$$

and

$$k = k_i + k_p n_\infty \tag{14}$$

On setting $s = 1$ at $t = 0$ and solving, we obtain

$$n_\infty = \frac{k_i}{k_p}\left(-1 + \left(\frac{2 + k_i/k_p}{k_i/k_p}\right)^{1/2}\right) \quad (15)$$

for n_∞, the inverse of the mean walk length, $\langle L\rangle$, at long times. The effective first-order rate constant, k, is given by

$$k = k_i(1 + 2\omega)^{1/2}; \qquad \omega = k_p/k_i \quad (16)$$

When the propagation step is slow, $k_p \rightarrow 0$, $n_\infty \rightarrow 1$, and $k \rightarrow k_i$. On the other hand, when the rate of initiation is low, $\omega = k_p/k_i \gg 1$; we can then obtain simple expressions

$$\langle L\rangle = 1/n_\infty = \left(\frac{k_p}{2k_i}\right)^{1/2} \quad \text{and} \quad k = (2k_ik_p)^{1/2} \quad (17)$$

for the mean random walk length and the effective first-order rate constant, k, describing the observed kinetics.

Equations 12 and 13 indicate that *after an induction period* (i.e., for $kt > 1$), the reaction will appear to follow first-order kinetics, $s \sim e^{-kt}$, as has been observed experimentally.[33,56,57] The mole fraction of carbon radicals on the surface, n, also shows first-order growth kinetics, $n = n_\infty(1 - e^{-kt})$, for $kt > 1$. The effective first-order rate constant, k, describing the observed kinetics (and the induction period before this behavior is established) is given by eq 16.

Under conditions where propagation is faster than initiation, $\omega \gg 1$, which are typical of the usual experimental situations, it is only possible to obtain the product k_ik_p by fitting eq 13 to experimental data because k_i does not appear separately in the expression for k. A separate determination of k_i requires either high precision data at either the very early stages of the reaction when the number of radicals on the surface can be detected directly, or high precision data at the end of the reaction when $s \sim e^{-k_it}$ (see the Appendix and the section on Monte Carlo simulation of the mechanism). Techniques such as the radical clock may be necessary to determine k_p directly.[68] However, eq 17 does show that the effective activation energy obtained from an Arrhenius plot of the experimental data will be the mean of the activation energies of the initiation and propagation steps, $E_{a,MF} = 0.5(E_i + E_p)$, assuming that each of these steps shows normal Arrhenius behavior.

Case III: Finite Termination Kinetics. When $k_t > 0$, n decays exponentially at sufficiently long times because $s \rightarrow 0$ and eq 7 then reduces to a simple first-order rate law with pseudo-first-order rate constant, k_t. In the course of the reaction, n therefore passes through a maximum before decaying to zero as the radicals are eventually lost via the termination reaction. If $k_t \ll k_i$, then for times such that $1/k < t < 1/k_t$ the maximum value of n is close to that given by eq 15. The kinetics are hardly affected by the termination reaction for these times and are therefore given by eqs 12 and 13 in the previous section: this is the case we observe experimentally for the thermal reaction of undecene with porous silicon reported below. If $k_t \cong k_i$, a significant deviation from first-order kinetics would have been observed (Figure 1), but for any $k_t > 0$ the long-time behavior of s is given by $s \sim e^{-k_it}$ (see Appendix).

Kinetic Model. Monte Carlo Simulation. The mean-field treatment described above neglects three important aspects of the problem: (i) some carbon radicals may have no nearest neighbor Si−H sites available even though $s > 0$; (ii) those Si−H sites which are surrounded by reacted sites can only react after a further initiation step; (iii) no account is taken of the structure of the surface. We have not been able to extend our treatment of the mechanism beyond the mean-field approximation by analytical methods. We therefore made a Monte Carlo simulation of the system to investigate the effect of these factors on the observed kinetics. These simulations are not an extension of the basic mechanism (1)−(4), rather they indicate the nature of the mathematical approximations inherent in eqs 7 and 8.

Previous workers have simulated the propagation step by treating it as a self-avoiding random walk.[10] That work addressed points i and iii by simulating a single random walk on the triangular lattice. Such a walk was found to last on average about 76 steps before terminating when the walk had looped back on itself in such a way that no unoccupied nearest neighbors were available. We have extended this approach to allow the simulation to model the effects due to interaction of many self-avoiding random walks, which are initiated at a rate dependent on the value of k_i and propagated at a rate determined by k_p. These simulations provide directly the mean random walk length $\langle L\rangle$ and the rate of consumption of Si−H sites when averages are taken over simulation spaces with dimensions much greater than $\langle L\rangle$.

A brief outline of the simulation algorithm consists of the following procedures at each time-step:

(1) Loop over all existing radicals and allow a chance[69] of $0 < k_p < 1$ that the radical center will propagate to a randomly selected nearest neighbor (if the neighboring site is already occupied, pass on to the next radical in the list).

(2) Loop over all lattice points and allow a chance $0 < k_i < 1$ for each unoccupied lattice point to become the site at which a new radical is initiated. Assume that an alkene adds immediately to form the corresponding carbon radical (eq 2).

To reduce finite size effects, periodic boundary conditions were imposed on the random walks and all the simulation results discussed were run on lattices of 1000×1000 points. Some simulations were run on a range of lattice sizes of $N \times N$ points where $N = 100$ to 1000 to reduce the statistical and finite-size errors. Through extrapolation of the simulation results against $1/N$, we estimate these errors for the largest lattice to be <2% on $s(t)$ and < 0.3% on $\langle L\rangle$ over the range of values of ω and t studied. The only cases where larger errors were found were for very long times when $\ln s < -6$ or for the case $\omega = 1$, $s < 10^{-1}$, which is not a situation of much experimental interest.

In imitation of the Si(111)−H and Si(100)−H surfaces we employed both triangular and rectangular lattices. On the rectangular lattice we restricted the walk to propagate along rows to model the formation of lines observed by previous workers in a scanning tunneling microscopy (STM) study of the reaction of styrene with Si(100)−H.[23,27] No such restriction was made on the triangular lattice because the available STM data for the Si(111)−H/styrene system shows the formation of two-dimensional structures rather than lines.[5,15,52]

Figure 2 shows kinetic data from simulations on the triangular lattice as a function of the ratio $\omega = k_p/k_i$ over the range $9 < \omega < 9000$. The simulation data are displayed in the form of the usual semilogarithmic plot of $\ln s$ against t which would be made to extract the apparent first-order rate constant from experimental data. Three distinct regions are observed in the curves: at short times the rate is low because few radicals are present; at intermediate times the graph is linear with a slope dependent on k_i and k_p; and at long times (e.g., in Figure 2b, $\ln s < -3$) another linear region with a slope equal to $-k_i$ is observed. The first two regions of Figure 2 are qualitatively the same as given by the mean-field treatment with $k_t = 0$ (Figure 1i), but the decrease in rate at long times is not. Equation 13 can be used to fit the simulation data for short and intermediate times, but the rate constant, k, obtained from the

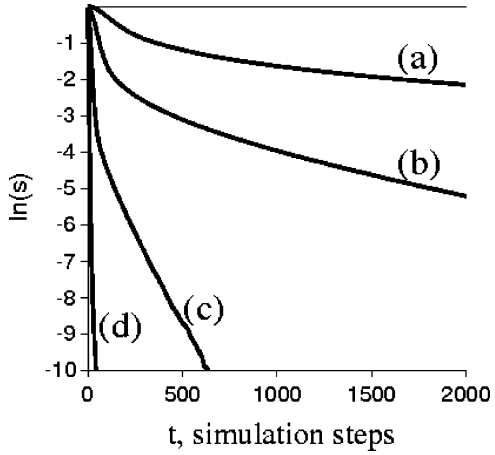

Figure 2. Simulation data for random walks on a triangular lattice modeling the mechanism of hydrosilation at Si(111)−H surfaces. The graph shows ln *s* versus *t* where *s* is the fraction of unreacted sites on the lattice and *t* is the number of Monte Carlo steps in the simulation. The ratio of the rate constants for propagation and initiation, $\omega = k_p/k_i$. In every case, $k_p = 0.9$ step^{-1} and (a) $\omega = 9000$, (b) $\omega = 900$, and (c) $\omega = 90$ and (d) $\omega = 9$.

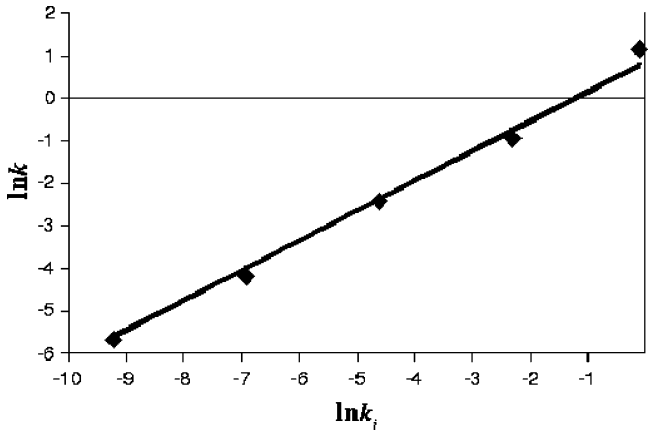

Figure 3. Plot of ln *k* versus ln k_i from the simulations of random walks on the triangular lattice (Figure 2). The slope of the best fit line shown is 0.7. *k* is the effective rate constant obtained from a linear fit to the intermediate time region in Figure 2.

fit is significantly less than that predicted by the mean-field treatment (eqs 14−17). The difference is due to crowding effects arising from interaction of many random walks on the surface which reduces $\langle L \rangle$ below the mean-field value and changes the dependence of *k* on ω as expected from eq 14.

Figure 3 plots the apparent first-order rate constants from the simulation against ω. We assumed the data could be described by a functional form, $k \sim k_i^{\alpha} k_p^{\beta}$, with $\alpha + \beta = 1$ on dimensional grounds. The first linear region of the simulated data can then be fitted by $\ln(s) = -kt$ with $k \propto k_i^{0.7} k_p^{0.3}$, which differs from the mean field prediction of $k \propto k_i^{0.5} k_p^{0.5}$. The corresponding values of the apparent activation energy from the Monte Carlo simulation ($E_{a,MC}$) and the mean-field treatment ($E_{a,MF}$) are $E_{a,MC} = (0.7E_i + 0.3E_p)$ and $E_{a,MF} = 0.5(E_i + E_p)$ where E_i and E_p are the activation energies of the initiation and propagation steps. This is discussed further in the section on density functional calculations of E_i and E_p and the experimental data for the reaction of undecene with porous silicon.

The second important result of the simulation in Figure 2 is that at long times the apparent first-order rate constant that would be determined by fitting a simple exponential to experimental data is k_i even when no chemical termination step is present. The reason for this switch in kinetic behavior is that at high

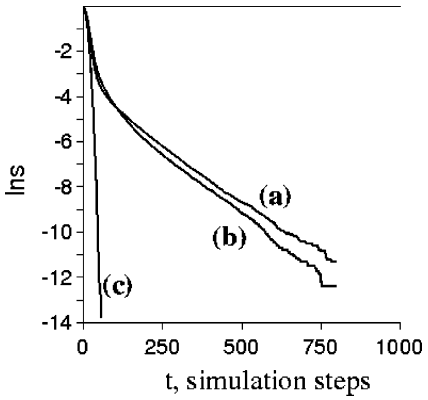

Figure 4. Simulations of the hydrosilation mechanism by random walks: (a) on a triangular lattice corresponding to Si(111)−H; (b) along the rows of a square lattice, but in random directions, corresponding to Si(100)/porous silicon; and (c) along rows, but in a fixed direction on each row. The fraction of unreacted sites is *s* and the time, *t*, is the number of Monte Carlo steps in the simulation. For every curve, the values of the initiation and propagation rate constants were $k_i = 0.01$ step^{-1} and $k_p = 0.9$ step^{-1}; $\omega = 90$.

coverages a significant fraction of the available surface sites are surrounded by occupied sites and cannot be accessed by a propagating random walk; these sites each require a separate initiation event to react. When these sites dominate, the kinetic behavior switches to the form $s \sim e^{-k_i t}$. The surface coverage at which this occurs depends on the mean length of the random walks and therefore on the ratio $\omega = k_p/k_i$; the required surface coverage decreasing as ω increases. For $\omega < 100$ the switch occurs at surface coverages (>95%) too close to a complete monolayer, to be easily observed experimentally. However, for $\omega \gg 1000$, this region could be resolved in the experimental data. Data on single-crystal Si(111)−H suggestive of such a switch in kinetics has in fact been reported.[33] Using attenuated total reflection Fourier transform infrared and vis−IR sum-frequency spectroscopy, these authors monitored the monolayer surface coverage and ordering with time. They observed first-order kinetics ($\ln s = -kt$) up to about 60% of a full monolayer and a decrease in rate thereafter. We agree that the spectroscopic data show convincingly the incomplete monolayers have less order but suggest that the change in ordering is not the sole cause of the subsequent decrease in rate, but rather that the slow-down is a natural feature of the mechanism. As shown in the Appendix, this behavior is also found when the radicals are lost by a termination process such as reaction 4.

Effect of Lattice Geometry. Figure 4 compares three simulations at the same value of $\omega = k_p/k_i$ to show the effect of the surface structure on the kinetics.

Figure 4a shows the results for the triangular lattice appropriate for the Si(111)−H surface and Figure 4b is a simulation in which the random walks are confined to a row of Si atoms in imitation of the experimental data for the Si(100)−H surface—the latter walks are random only in the sense that each has a randomly determined direction.[70] Finally, as illustrated in Scheme 1, Figure 4c is a simulation where the "random" walk on any particular row is artificially forced to proceed in one direction.

Qualitatively the behavior in simulations a and b in Figure 4 is the same: after an induction period, $\ln s \sim -kt$ until $\ln s < -3$, and then the rate slows to give at long times $\ln s \sim -k_i t$. In Figure 4c this switch in kinetics is not observed. The reason for this is that when the propagation step is constrained to run in one direction along any particular row, there is no possibility to create unreacted Si−H sites which are surrounded by reacted

SCHEME 1. Schematic of Three Different Types of Monolayer Growth Simulated[a]

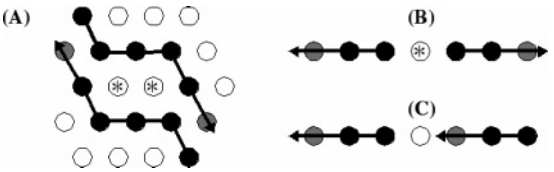

[a] (A) random walks on a triangular lattice [Si(111)], (B) walks along a row of the Si(100) surface in which the direction of any particular walk is not specified, and (C) walks along a row of the Si(100) surface in which all walks are in the same direction on a given row. The open circles represent unreacted Si−H sites, the black circles represent reacted Si−alkyl sites, and the gray circles represent the radical chain center at which the reaction propagates as indicated by the arrows. Asterisks (*) mark Si−H sites which are inaccessible to the propagation steps and may only react if a new walk is initiated at these sites. No such cases are possible for (C), but in (A) and (B) accumulation of such * sites leads to the switch in kinetic behavior at long times discussed in the text.

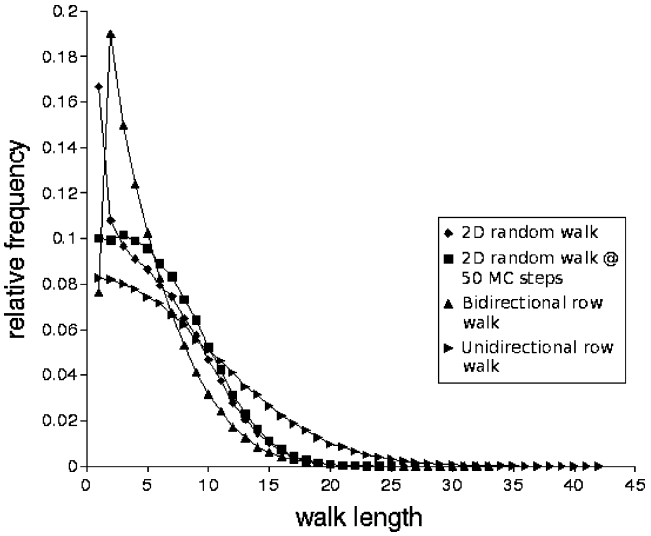

Figure 5. Simulated distributions of random walk lengths during monolayer formation under various conditions. The relative frequency of random walks of a particular length (measured in numbers of surface sites) is shown for (i) 2D self-avoiding random walks on a triangular lattice, as in Figure 4a, at complete reaction diamonds; (ii) 2D self-avoiding random walk on a triangular lattice after 50 Monte Carlo steps (squares); (iii) walks restricted to proceed along rows, but in either direction as in Figure 4b and Scheme 1b (triangles-up); and (iv) walks restricted to rows and a specified direction on any particular row as in Figure 4c and Scheme 1c (triangles-right). $k_i = 0.01$ step^{-1}, $\omega = 90$, and $k_p = 0.9$ step^{-1} in all cases.

sites and inaccessible to all radicals on the surface. This clearly demonstrates the origin of the switch in kinetic behavior observed in simulations a and b in Figure 4 which is due to the slow process of initiating new radicals in the holes in the monolayer that are surrounded (see Scheme 1). Figure 5 shows the effect of this switch in behavior on the distribution of random walk lengths. The distributions shown are those at the end of the reaction ($s = 0$) and in one example at an earlier time just before the switch in kinetics from $\ln s \sim -kt$ to $\ln s \sim -k_i t$. If the distribution is observed before the switch in kinetics, or at complete reaction for the case (Figure 4c) where there is no switch in kinetic behavior, then the distribution is relatively flat for short walk lengths and decays monotonically for larger walk lengths. However, after the switch in kinetic behavior a marked increase in the relative frequency of short walks is observed—illustrating that the later stages of the reaction correspond to

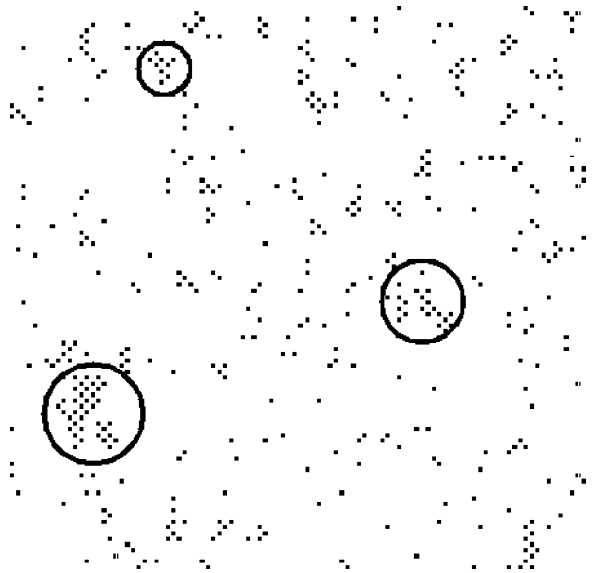

Figure 6. Snapshot of a 100 × 100 site portion of the lattice [Si(111)] after 250 steps of the Monte Carlo simulation with $\omega = 900$. The white regions correspond to reacted sites, and the black squares are empty lattice sites. A few larger clusters of these empty sites are circled, but the majority of unreacted sites at long times are small clusters or individual isolated sites of the type indicated in Scheme 1.

the filling-in of small holes. This process requires a separate initiation step for each small hole; hence $\ln s \sim -k_i t$. In typical experimental situations, a sample removed from the reaction and examined by probe microscopy will always contain some small holes in the monolayer that are not yet filled because of the slow-down in the kinetics.

Pinholes. The simulations suggest that pinhole defects will be present in these monolayers and can only be removed at long reaction times. Figure 6 shows a snapshot of a simulation of the Si(111) surface for $\omega = 900$ after 250 steps; this corresponds to a time at which the change in kinetic behavior is occurring (see Figure 2b). The white regions correspond to reacted sites and those sites not part of the triangular lattice are also colored white. The black squares are empty, unreacted sites and the majority of these are isolated single molecule sites, but there are a significant number of larger clusters (circled). Pinholes also occur in Au−thiolate self-assembled monolayers (SAMs), but their nature and origin are different. The Si−C bond is not labile and there is no similar mechanism for annealing of the Si−C-based SAMs.

Comparison with Experimental Kinetic Data for the Thermal Hydrosilation Reaction of Alkenes on Porous Silicon. Previous kinetic data on the reaction of undecene with porous silicon showed that FTIR spectroscopy can be used to observe the first-order kinetics by monitoring ex situ the extent of alkylation of the surface as a function of reaction time.[56] However, to observe the detailed kinetics of the reaction described by eqs 12−16, many more measurements and greater precision are required. We therefore altered the experimental protocol to study the thermal reaction of 1-undecene with porous silicon under reflux at a controlled temperature and with many more data points on each kinetic run. Through the use of mixtures of toluene and ethylbenzene we varied the reaction temperature over the range 111−136 °C. The extent of reaction was monitored by integrating the C−H stretching bands observed between 3000 and 2850 cm^{-1}. The fraction of unreacted sites, s, is therefore proportional to the difference in the integrated C−H intensity at completion and at time t; $A(\infty) - A(t)$.

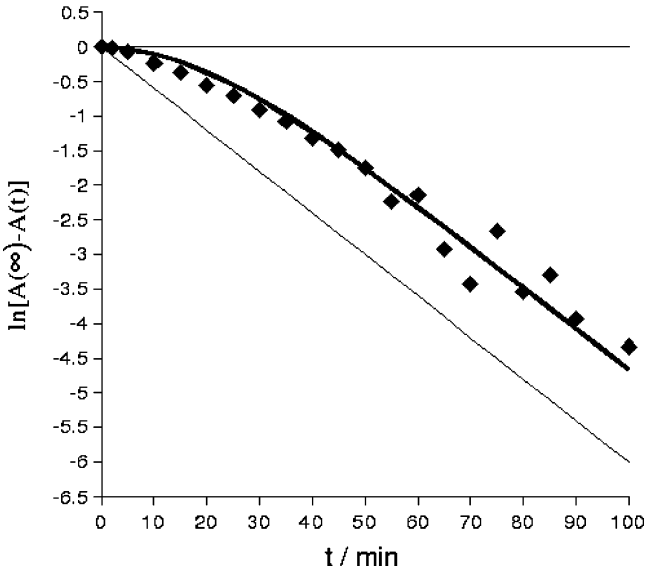

Figure 7. Experimental kinetic data for the thermal reaction of undecene (100 mM) with porous silicon in refluxing toluene. $A(\infty) - A(t)$ is the difference in the integrated C−H intensity at completion and at time *t*. The amount of alkyl species on the porous silicon surface was obtained by integrating the bands due to C−H stretching modes in the FTIR spectrum over the range 2850−3000 cm^{-1}. The effective first-order rate constant corresponding to the linear portion of the graph is $k = 0.06$ min^{-1}. The bold line is the result of fitting eqs 12−16 to the data and the thin line is a guide to the eye showing a simple exponential, $\exp(-kt)$.

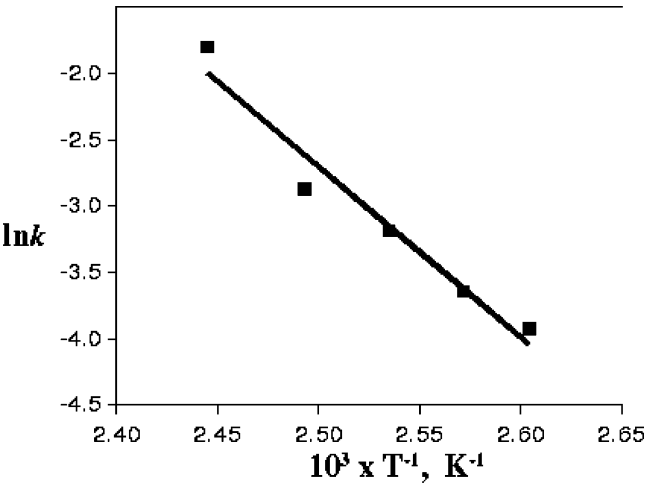

Figure 8. Arrhenius plot for the effective first-order rate constant, *k*, of the reaction of undecene with porous silicon at reflux in mixtures of toluene and ethylbenzene.

Figure 7 shows the usual semilogarithmic plot for first-order kinetics and the fit of the kinetic model (ignoring any termination reaction) as described by eqs 12−16. It can clearly be seen that the experimental data are not described by a simple exponential over the whole range of times: there is an induction period (ca. 15−20 min) before first-order kinetics are observed and we obtained $k = 0.06$ min^{-1} from the fit. However, it is not possible to extract reliable values of k_i and k_p individually from the experimental data because this requires high precision data either at very short times where $A(t)$ is small (see Appendix) or at very long times to observe the switch in kinetic behavior when $A(\infty) - A(t)$ is very small. Instead, we compared the activation energy obtained by determining *k* at various temperatures (Figure 8) to calculations of the transition states for initiation and propagation obtained by density functional methods (Table 1).

TABLE 1: Comparison of Calculated and Experimental Activation Energies for Reaction of Alkenes with Hydrogen-Terminated Silicon[a]

computed activation energy (MF), kJ mol^{-1}	computed activation energy (MC), kJ mol^{-1}	activation energy (experiment, data of Figure 8), kJ mol^{-1}
103.8 (98.5)	117.7 (110.4)	106.9

[a] The experimental data are for undecene/porous silicon. The activation energy for the abstraction of hydrogen by oxygen (E_i) was that calculated for the Si_6 cluster in this work (B3LYP/6-31G(d,p), ROHF). The activation energy of the propagation step (E_p) is taken from the study of Si(111)−H/C_2H_4 reported by Takeuchi et al.[55] MF indicates that the mean-field expression, $E_{a,MF} = 0.5(E_i + E_p)$ was used to calculate the overall activation energy of the reaction and MC indicates that the expression for the overall activation energy from the Monte Carlo simulations, $E_{a,MC} = (0.7E_i + 0.3E_p)$, was used. E_i and E_p denote the activation energies of the initiation and propagation steps. Values in parentheses were calculated using the enthalpy of activation for the initiation step—enthalpies are not available for the calculations of the propagation step on large clusters.

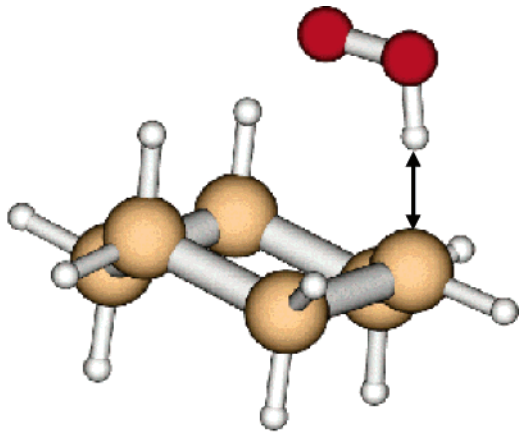

Figure 9. Transition state for the initiation reaction in which oxygen abstracts a hydrogen atom from the surface, modeled by an Si_6H_{12} cluster (B3LYP/6-31G(d,p), ROHF). The double-headed arrow is a guide to the eye which indicates the reaction coordinate.

Density Functional Calculations of the Activation Energy. Several workers have previously reported calculations of the propagation transition state,[52,55,62] and a range of values including 62.6 kJ mol^{-1} using an Si_{12} cluster with fixed Si atoms[62] and 68.8 kJ mol^{-1} using a larger slab of Si[55] have been obtained. The activation energies for propagation along a line on the Si(100) surface during reaction of propene, styrene, vinylferrocene, and longer alk-1-enes have also been calculated with density functional methods.[53,54,68,71] The propagation step appears to be favored for longer alkenes because dispersion interactions disfavor desorption of the carbon radical while a similar activation energy for propagation (undecene ∼ 0.7 eV, 67.5 kJ mol^{-1}) to those given above was obtained.[53] To our knowledge, the initiation step has previously been computed only as an Si−H bond scission (330−350 kJ mol^{-1} [62,63]) and values for abstraction of the H atom by oxygen are not available.

The molecular model ($Si_6H_{12} + O_2$) of the initiation step computed here comprises a ring of six Si atoms in the chair conformation to simulate the geometry of the Si(111) surface.

We calculated the energy and normal modes of the reactants at their equilibrium geometry and at the first-order saddle point (Figure 9). This transition state was verified by inspection of the normal modes to correspond to abstraction of a H atom by oxygen. The normal-mode analysis confirmed that the frequencies of every mode were real for the reactant geometries, and we observed a single imaginary frequency corresponding to a

path connecting reactants and products for the calculated transition state. The internal energy of activation was 128 kJ mol^{-1}, and the enthalpy of activation was 139 kJ mol^{-1}. These values were combined with literature calculations for the propagation step, and the overall activation energy for the reaction is compared to the experimental value in Table 1.

The theoretical values of activation energy were calculated using the expressions $E_{a,MC} = (0.7E_i + 0.3E_p)$ and $E_{a,MF} = 0.5(E_i + E_p)$ obtained from the Monte Carlo simulations and the mean-field treatment. The activation energy for abstraction of a hydrogen atom by oxygen is much lower (128−139 kJ mol^{-1}) than that obtained by Si−H bond scission (330−350 kJ mol^{-1} [62,63]). Reasonable agreement between the calculated and measured values is also obtained, and this supports our suggestion that the initiation step is abstraction of a hydrogen atom from an Si−H site by trace oxygen.[51]

Conclusions

A kinetic model for the formation of organic monolayers on hydrogen-terminated silicon has been analyzed. The model is based on a previously proposed and widely discussed mechanism (ref 2): After an initiation step, the silyl radical produced attacks the alkene forming an Si−C bond and the radical at the β-carbon then propagates by abstracting a hydrogen atom from the nearest-neighbor Si−H site. A solution to the corresponding mean-field kinetic equations was obtained which can be used to fit experimental kinetic data to obtain the product of the rate constants for the initiation and propagation steps. FTIR data for the reaction of undecene with porous silicon are in agreement with the qualitative features of the mean-field treatment, an induction period followed by first-order kinetics with an effective rate constant dependent on the rate constants, k_i and k_p, for both the initiation and propagation steps. At long times the model predicts the rate decreases, and the effective first-order rate constant becomes k_i. Monte Carlo simulations show this occurs, even in the absence of an explicit chemical termination step, because the kinetics are now determined by the filling-in of the small holes in the monolayer. The simulations also indicate the rate constant for growth of the monolayer is $k \propto k_i^{0.7}k_p^{0.3}$, and therefore the activation energy obtained from the experimental data is $E_{a,MC} = (0.7E_i + 0.3E_p)$ compared to the mean-field prediction of $E_{a,MF} = 0.5(E_i + E_p)$. DFT calculations of the transition states for initiation and propagation were found to predict an activation energy in reasonable agreement with experiment.

Acknowledgment. The EPSRC and BBSRC (B.R.H./A.H.), ESPOM (S.C.), and The Research Council of Norway (L.H.L.) are thanked for funding. The help of Sebastian Del Bano and Geoffrey Horrocks is acknowledged.

Appendix A Linear approximations

Although a closed-form solution was not obtained for the model when $k_t > 0$, we can obtain asymptotic expressions for s and n by making a Taylor expansion of the right-hand sides of eqs 7 and 8 around various known points and retaining terms up to first order in s and n.

1. Long Times as $n, s \rightarrow 0$. Equations 7 and 8 can be linearized around $n = 0$, $s = 0$, and the resulting system is

$$\frac{dn}{dt} = k_i s - k_t n \tag{A1}$$

$$\frac{ds}{dt} = -k_i s \tag{A2}$$

The same equations are obtained if we treat the termination process as being due to the radical becoming surrounded by reacted sites and approximate the termination rate by $k_t n(1 - s)$. Where the factor $(1 - s)$ is the mean fraction of reacted nearest neighbor sites. The solution

$$s = s_0 e^{-k_i t}$$

$$n = n_0 e^{-k_i t} + \frac{k_i s_0}{k_t - k_i}[e^{-k_i t} - e^{-k_t t}] \tag{A3}$$

decays exponentially at long times for both s and n. Note that the effective first-order rate constant for the decay of s is k_i.

Making a similar linearization for the case $k_t = 0$ requires a Taylor expansion around $s = 0$, $n = n_\infty$ because $dn/dt \rightarrow 0$ as $t \rightarrow \infty$. The system then reduces to the first-order equation

$$\frac{ds}{dt} = -k_i s - k_p n_\infty s \tag{A4}$$

and the solution is simply $s = s_0 e^{-kt}$; $k = k_i + k_p n_\infty$. When the rate of termination, reaction 4, is finite, then $n \rightarrow 0$ and the last few sites on the surface require fresh radicals to be initiated via reaction 1. However, when the termination rate (4) is zero, the propagation step, reaction 3, continues until all the sites are exhausted. Nevertheless even when the termination rate is finite, similar behavior to eq A4 is observed at intermediate times when n passes through its maximum value, n_m. The corresponding linearization at this point leads to $s = s_0 e^{-kt}$; $k = k_i + k_p n_m$ and for sufficiently small k_t, $n_m \cong n_\infty$.

When the mean-field approximation is abandoned, the simulation data show that at long times a few unreacted sites on the surface are surrounded by reacted sites and cannot be accessed by propagation steps even when $k_t = 0$. This effect is therefore difficult to distinguish from that of a small, finite rate of chemical termination in a purely kinetic experiment (but may be seen in probe microscopy) because both result in a switch from $s \sim e^{-kt}$ to $s \sim e^{-k_i t}$ at sufficiently long times as shown above.

2. Short Times as $n \rightarrow 0$ and $s \rightarrow 1$. If instead we linearize around $n = 0$, $s = 1$, then eqs 7 and 8 reduce to

$$\frac{dn}{dt} = k_i s - k_t n \tag{A5}$$

and

$$\frac{ds}{dt} = -k_i s - k_p n \tag{A6}$$

These equations are conveniently solved by taking Laplace transforms (p is the Laplace variable and $\underline{n}$ and $\underline{s}$ are the transforms of n and s) to obtain

$$(p + k_t)\underline{n} = k_i \underline{s} + n(0) \tag{A7}$$

and

$$(p + k_i)\underline{s} = s(0) - k_p \underline{n} \tag{A8}$$

$\underline{n}$ and $\underline{s}$ are given by

$$\underline{n} = \frac{k_i}{p^2 + (k_i + k_t)p + k_i(k_p + k_t)} \tag{A9}$$

and

$$\underline{s} = \frac{p + k_t}{p^2 + (k_i + k_t)p + k_i(k_p + k_t)} \tag{A10}$$

Under the assumption that $k_p \gg k_i$ and k_t, the solutions for n and s after inverting the Laplace transforms and ignoring terms containing k_p in the denominator are

$$n \cong \left(\frac{k_i}{k_p}\right)^{1/2} e^{-(1/2)(k_i+k_t)t} \sin(k_i k_p)^{1/2} t \tag{A11}$$

and

$$s \cong e^{-(1/2)(k_i+k_t)t} \cos(k_i k_p)^{1/2} t \tag{A12}$$

This linearization applies in the neighborhood of $t = 0$, i.e., for $(k_i k_p)^{1/2} t \ll 1$. The important terms in eqs A11 and A12 are therefore

$$n \sim k_i t \tag{A13}$$

and

$$s \sim e^{-(1/2)(k_i+k_t)t} \tag{A14}$$

Conclusion. We can summarize the behavior of the system given by eqs 7 and 8, as follows: (i) the short time solution is determined by k_i and k_t; (ii) at intermediate times $s \sim e^{-kt}$; $k = k_i + k_p n_m$; (iii) at long times $s \sim e^{-k_i t}$. If $k_t = 0$, then the long time behavior is $s \sim e^{-kt}$; $k = k_i + k_p n_\infty$ although this applies only within the mean field approximation.

References and Notes

(1) Linford, M. R.; Chidsey, C. E. D. *J. Am. Chem. Soc.* **1993**, *115*, 12631.

(2) Linford, M. R.; Fenter, P.; Eisenberger, P. M.; Chidsey, C. E. D. *J. Am. Chem. Soc.* **1995**, *117*, 3145.

(3) Buriak, J. M. *Chem. Rev.* **2002**, *102*, 1271.

(4) Sieval, A. B.; Linke, R.; Zuilhof, H.; Sudholter, E. J. R. *Adv. Mater.* **2000**, *12*, 1457.

(5) Wayner, D. D. M.; Wolkow, R. A. *J. Chem. Soc., Perkin Trans. 2* **2002**, 23.

(6) Sung, M. M.; Kluth, G. J.; Yauw, O. W.; Maboudian, R. *Langmuir* **1997**, *13*, 6164.

(7) Bateman, J. E.; Eagling, R. D.; Worrall, D. R.; Horrocks, B. R.; Houlton, A. *Angew. Chem., Int. Ed.* **1998**, *37*, 2683.

(8) Boukherroub, R.; Wojtyk, J. T. C.; Wayner, D. D. M.; Lockwood, D. J. *J. Electrochem. Soc.* **2002**, *149*, H59.

(9) Sieval, A. B.; Vleeming, V.; Zuilhof, H.; Sudholter, E. J. R. *Langmuir* **1999**, *15*, 8288.

(10) Cicero, R. L.; Linford, M. R.; Chidsey, C. E. D. *Langmuir* **2000**, *16*, 5688.

(11) Effenberger, F.; Gotz, G.; Bidlingmaier, B.; Wezstein, M. *Angew. Chem., Int. Ed.* **1998**, *37*, 2462.

(12) Stewart, M. P.; Buriak, J. M. *J. Am. Chem. Soc.* **2001**, *123*, 7821.

(13) de Smet, L. C. P. M.; Stork, G. A.; Hurenkarnp, G. H. F.; Sun, Q. Y.; Topal, H.; Vronen, P. J. E.; Sieval, A. B.; Wright, A.; Visser, G. M.; Zuilhof, H.; Sudholter, E. J. R. *J. Am. Chem. Soc.* **2003**, *125*, 13916.

(14) Sun, Q. Y.; de Smet, L. C. P. M.; van Lagen, B.; Wright, A.; Zuilhof, H.; Sudholter, E. J. R. *Angew. Chem., Int. Ed.* **2004**, *43*, 1352.

(15) Eves, B. J.; Sun, Q. Y.; Lopinski, G. P.; Zuilhof, H. *J. Am. Chem. Soc.* **2004**, *126*, 14318.

(16) Sun, Q. Y.; de Smet, L. C. P. M.; van Lagen, B.; Giesbers, M.; Thune, P. C.; van Engelenburg, J.; de Wolf, F. A.; Zuilhof, H.; Sudholter, E. J. R. *J. Am. Chem. Soc.* **2005**, *127*, 2514.

(17) Zazzera, L. A.; Evans, J. F.; Deruelle, M.; Tirrell, M.; Kessel, C. R.; McKeown, P. *J. Electrochem. Soc.* **1997**, *144*, 2184.

(18) Buriak, J. M.; Allen, M. J. *J. Am. Chem. Soc.* **1998**, *120*, 1339.

(19) Schmeltzer, J. M.; Porter, L. A.; Stewart, M. P.; Buriak, J. M. *Langmuir* **2002**, *18*, 2971.

(20) Saghatelian, A.; Buriak, J.; Lin, V. S. Y.; Ghadiri, M. R. *Tetrahedron* **2001**, *57*, 5131.

(21) Robins, E. G.; Stewart, M. P.; Buriak, J. M. *Chem. Commun.* **1999**, 2479.

(22) Hurley, P. T.; Ribbe, A. E.; Buriak, J. M. *J. Am. Chem. Soc.* **2003**, *125*, 11334.

(23) Lopinski, G. P.; Wayner, D. D. M.; Wolkow, R. A. *Nature* **2000**, *406*, 48.

(24) Kruse, P.; Johnson, E. R.; DiLabio, G. A.; Wolkow, R. A. *Nano Lett.* **2002**, *2*, 807.

(25) Tong, X.; DiLabio, G. A.; Wolkow, R. A. *Nano Lett.* **2004**, *4*, 979.

(26) Tong, X.; DiLabio, G. A.; Clarkin, O. J.; Wolkow, R. A. *Nano Lett.* **2004**, *4*, 357.

(27) Pitters, J. L.; Wolkow, R. A. *J. Am. Chem. Soc.* **2005**, *127*, 48.

(28) Strother, T.; Cai, W.; Zhao, X.; Hamers, R. J.; Smith, L. M. *J. Am. Chem. Soc.* **2000**, *122*, 1205.

(29) Pike, A. R.; Lie, L. H.; Eagling, R. A.; Ryder, L. C.; Patole, S. N.; Connolly, B. A.; Horrocks, B. R.; Houlton, A. *Angew. Chem., Int. Ed.* **2002**, *41*, 615.

(30) Sieval, A. B.; Demirel, A. L.; Nissink, J. W. M.; Linford, M. R.; van der Maas, J. H.; de Jeu, W. H.; Zuilhof, H.; Sudholter, E. J. R. *Langmuir* **1998**, *14*, 1759.

(31) Sieval, A. B.; van den Hout, B.; Zuilhof, H.; Sudholter, E. J. R. *Langmuir* **2000**, *16*, 2987.

(32) Ishibashi, T.; Ara, M.; Tada, H.; Onishi, H. *Chem. Phys. Lett.* **2003**, *367*, 376.

(33) Quayum, M. E.; Kondo, T.; Nihonyanagi, S.; Miyamoto, D.; Uosaki, K. *Chem. Lett.* **2002**, 208.

(34) Nihonyanagi, S.; Miyamoto, D.; Idojiri, S.; Uosaki, K. *J. Am. Chem. Soc.* **2004**, *126*, 7034.

(35) Allongue, P.; de Villeneuve, C. H.; Pinson, J. *Electrochim. Acta* **2000**, *45*, 3241.

(36) Yu, H. Z.; Morin, S.; Wayner, D. D. M.; Allongue, P.; de Villeneuve, C. H. *J. Phys. Chem. B* **2000**, *104*, 11157.

(37) Fidélis, A.; Ozanam, F.; Chazalviel, J.-N. *Surf. Sci. Lett.* **2000**, *L7*, 444.

(38) Sieval, A. B.; Opitz, R.; Maas, H. P. A.; Schoeman, M. G.; Meijer, G.; Vergeldt, F. J.; Zuilhof, H.; Sudholter, E. J. R. *Langmuir* **2000**, *16*, 10359.

(39) Nealey, P. F.; Black, A. J.; Wilbur, J. L.; Whitesides, G. M. In *Molecular Electronics*; Jortner, J., Ratner, M. A., Eds.; Blackwell Science Ltd.: Oxford, U.K., 1997; Chapter 11, pp 343−368.

(40) Buriak, J. M. *Chem. Commun.* **1999**, 1051.

(41) Gurtner, C.; Wun, A. W.; Sailor, M. J. *Angew. Chem., Int. Ed.* **1999**, *38*, 1966.

(42) Song, J. H.; Sailor, M. J. *Comments Inorg. Chem.* **1999**, *21*, 69 Part A.

(43) Sailor, M. J.; Lee, E. J. *Adv. Mater.* **1997**, *9*, 783.

(44) Lie, L. H.; Duerdin, M.; Tuite, E. M.; Houlton, A.; Horrocks, B. R. *J. Electroanal. Chem.* **2002**, *538*, 183.

(45) Lie, L. H.; Patole, S. N.; Pike, A. R.; Ryder, L. C.; Connolly, B. A.; Ward, A. D.; Tuite, E. M.; Houlton, A.; Horrocks, B. R. *Faraday Discuss.* **2004**, *125*, 235.

(46) Wang, L.; Reipa, V.; Blasic, J. *Bioconjugate Chem.* **2004**, *15*, 409.

(47) Li, X.; He, Y.; Swihart, M. T. *Langmuir* **2004**, *20*, 4720.

(48) Warner, J. H.; Hoshino, A.; Yamamoto, K.; Tilley, R. D. *Angew. Chem., Int. Ed.* **2005**, *44*, 4550.

(49) Stewart, M. P.; Buriak, J. M. *Angew. Chem., Int. Ed.* **1998**, *37*, 3257.

(50) Bateman, J. E.; Eagling, R. D.; Horrocks, B. R.; Houlton, A. *J. Phys. Chem. B* **2000**, *104*, 5557.

(51) de Smet, L. C. P. M.; Zuilhof, H.; Sudholter, E. J. R.; Lie, L. H.; Houlton, A.; Horrocks, B. R. *J. Phys. Chem. B* **2005**, *109*, 12020.

(52) Cicero, R. L.; Chidsey, C. E. D.; Lopinski, G. P.; Wayner, D. D. M.; Wolkow, R. A. *Langmuir* **2002**, *18*, 305.

(53) DiLabio, G. A.; Piva, P. G.; Kruse, P.; Wolkow, R. A. *J. Am. Chem. Soc.* **2004**, *126*, 16048.

(54) Kruse, P.; Johnson, E. R.; DiLabio, G. A.; Wolkow, R. A. *Nano Lett.* **2002**, *2*, 807.

(55) Takeuchi, N.; Kanai, Y.; Selloni, A. *J. Am. Chem. Soc.* **2004**, *126*, 15890.

(56) de Smet, L. C. P. M.; Zuilhof, H.; Sudholter, E. J. R.; Wittstock, G.; Duerdin, M. S.; Lie, L. H.; Houlton, A.; Horrocks, B. R. *Electrochim. Acta* **2002**, *47*, 2653.

(57) Kosuri, M. R.; Gerung, H.; Li, Q.; Han, S. M. *Langmuir* **2003**, *19*, 9315.

(58) Fellah, S.; Teyssot, A.; Ozanam, F.; Chazalviel, J.-N.; Vigneron, J.; Etcheberry, A. *Langmuir* **2002**, *18*, 5851.

(59) PC-GAMESS: Granovsky, A. A. http://classic.chem.msu.su/gran/gamess/index.html

(60) GAMESS: Schmidt, M. W.; Baldridge, K. K.; Boatz, J. A.; Elbert, S. T.; Gordon, M. S.; Jensen, J. J.; Koseki, S.; Matsunaga, N.; Nguyen, K. A.; Su, S.; Windus, T. L.; Dupuis, M.; Montgomery, J. A. *J. Comput. Chem.* **1993**, *14*, 1347.

(61) Scott, A. P.; Radom, L. *J. Phys. Chem.* **1996**, *100*, 16502.

(62) Pei, Y.; Ma, J.; Jiang, Y. *Langmuir* **2003**, *19*, 7652.

(63) Laarhoven, L. J. J.; Mulder, P.; Wayner, D. D. M. *Acc. Chem. Res.* **1999**, *32*, 342.

(64) Nising, P.; Meyer, T. *Ind. Eng. Chem. Res.* **2004**, *43*, 7220.

(65) Sieval, A. B.; van den Hout, B.; Zuilhof, H.; Sudholter, E. J. R. *Langmuir* **2001**, *17*, 2172.

(66) Wallart, X.; de Villeneuve, C. H.; Allongue, P. *J. Am. Chem. Soc.* **2005**, *127*, 7871.

(67) When $k_t = 0$, eqs 7 and 8 become equivalent to the second-order equation $n'' = -k_i n' - k_p nn'$. This can be integrated directly using $2nn' = (n^2)'$.

(68) Tong, X.; DiLabio, G. A.; Clarkin, O. J.; Wolkow, R. A. *Nano Lett.* **2004**, *4*, 357.

(69) The pseudorandom number generator used was "ran2" with a period $>2 \times 10^{18}$ from Chapter 7, section 7.1 of: Press, W. H.; Teukolsky, S. A.; Vetterling, W. T.; Flannery, B. P. *Numerical Recipes in Fortran*; *The Art of Scientific Computing*, 2nd ed.; Cambridge University Press: Cambridge, U.K., 1992.

(70) Clearly if the reaction is confined to a row of Si atoms, it cannot turn back on itself, but the initial direction of propagation immediately after initiation is equally likely to be left or right in the absence of reacted nearest neighbor sites.

(71) Tong, X.; DiLabio, G. A.; Wolkow, R. A. *Nano Lett.* **2004**, *4*, 979.